Acta Pharmaceutica Sinica B 2022;12(1):364–377

Chinese Pharmaceutical Association
Institute of Materia Medica, Chinese Academy of Medical Sciences

Acta Pharmaceutica Sinica B

www.elsevier.com/locate/apsb
www.sciencedirect.com

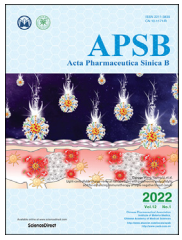

ORIGINAL ARTICLE

The osteogenic niche-targeted arsenic nanoparticles prevent colonization of disseminated breast tumor cells in the bone

Cong Liu[a,†], Anzhi Hu[a,†], Huijuan Chen[a], Jing Liang[b], Mancang Gu[a], Yang Xiong[a], Chao-Feng Mu[a,c,*]

[a]*School of Pharmaceutical Sciences, Zhejiang Chinese Medical University, Hangzhou 310053, China*
[b]*Center for Synthetic Biochemistry, Shenzhen Institute of Synthetic Biology, Shenzhen Institutes of Advanced Technology, Chinese Academy of Sciences, Shenzhen 518055, China*
[c]*Engineering Research Center of Clinical Functional Materials and Diagnosis & Treatment Devices of Zhejiang Province, Wenzhou Institute of Biomaterials and Engineering, Wenzhou 325011, China*

Received 11 March 2021; received in revised form 19 May 2021; accepted 24 May 2021

KEY WORDS

Bone metastasis;
Osteogenic niche;
Breast cancer;
Arsenic trioxide;
Bone marrow;
Bone colonization;
Arsenic-manganese nanocrystal;
Immature hydroxyapatite

Abstract Up to 70% of patients with late-stage breast cancer have bone metastasis. Current treatment regimens for breast cancer bone metastasis are palliative with no therapeutic cure. Disseminated tumor cells (DTCs) colonize inside the osteogenic niches in the early stage of bone metastasis. Drug delivery into osteogenic niches to inhibit DTC colonization can prevent bone metastasis from entering its late stage and therefore cure bone metastasis. Here, we constructed a 50% DSS6 peptide conjugated nanoparticle to target the osteogenic niche. The osteogenic niche was always located at the endosteum with immature hydroxyapatite. Arsenic-manganese nanocrystals (around 14 nm) were loaded in osteogenic niche-targeted PEG-PLGA nanoparticles with an acidic environment-triggered arsenic release. Arsenic formulations greatly reduced 4T1 cell adhesion to mesenchymal stem cells (MSCs)/preosteoblasts (pre-OBs) and osteogenic differentiation of osteoblastic cells. Arsenic formulations also prevented tumor cell colonization and dormancy *via* altering the direct interaction between 4T1 cells and MSCs/pre-OBs. The chemotactic migration of 4T1 cells toward osteogenic cells was blocked by arsenic in mimic 3D osteogenic niche. Systemic administration of osteogenic niche-targeted arsenic nanoparticles significantly extended the survival of mice with 4T1 syngeneic bone metastasis. Our findings provide an effective approach for osteogenic niche-specific drug delivery and suggest that bone metastasis can be effectively inhibited by blockage of tumor cell colonization in the bone microenvironment.

*Corresponding author. Tel./fax: +86 571 61768136.
E-mail address: cmu2005@126.com (Chao-Feng Mu).
[†]These authors made equal contributions to this work.
Peer review under responsibility of Chinese Pharmaceutical Association and Institute of Materia Medica, Chinese Academy of Medical Sciences.

https://doi.org/10.1016/j.apsb.2021.06.012

1. Introduction

Breast cancer is the most common malignant tumor in women. It is highly invasive and always associated with distant recurrence. About 70%−85% of patients with advanced breast cancer have bone metastasis. It's incurable once it reaches the late stage. Bone metastasis is a multi-step process and is mainly divided into four stages (colonization, survival and dormancy, reactivation, and growth)[1]. The current treatment strategies in the clinic, including chemotherapy, hormonal therapy, and using bone resorption inhibitors improve patient quality of life, but fail to prolong the overall survival in the late stage of bone metastasis, in which the "vicious cycle" has already established[2].

The bone metastasis process can be hindered if the colonization of breast cancer cells is inhibited in the initial stage. The local bone microenvironment before bone metastasis, known as the pre-metastatic niche, is generally a transient pro-inflammatory microenvironment driven by the primary tumor[3]. The bone marrow microvessels and the adjacent bone microenvironment (composed of mesenchymal stem cells, osteoblasts, and extracellular matrix) attract and guide disseminated tumor cells (DTCs) to the osteogenic niche, thereby facilitating tumor cells to colonize in the bone marrow[4,5]. The initiation of cancer cell colonization in bone is regulated by the local specific chemokines and adhesion molecules in the osteogenic niche. These secreted factors mainly refer to C−X−C motif chemokine ligand 12 (CXCL12), osteopontin (OPN), bone sialoprotein (BSP), and N-cadherin expressed by mesenchymal cells or osteoblast lineage cells adjacent to bone surfaces[6,7]. Bone metastasis can be avoided by rectifying the formed pre-metastatic osteogenic niche and preventing DTC colonization in the initial stage.

Where are the pre-metastatic osteogenic niches in the bone marrow? They do not distribute throughout the bone marrow. The latest animal studies have shown that breast cancer cells preferentially colonize the proximal tibial metaphysis, which contains immature hydroxyapatite (HA) with less-perfect and less-oriented crystals[8]. These immature HAs are new bone constituents produced by osteogenic cells in the osteogenic niches. Meanwhile, it has been observed that the most common sites of bone metastasis occur in the trabecular bone-rich spine, pelvis, and ribs with an active remodeling in the clinic[9,10]. These observations from experimental animal models and clinical samples show that the pre-metastatic osteogenic niches always locate at the endosteum of cancellous bone with high bone turnover.

It was reported that arsenic trioxide suppressed the interaction of cancer cells with the bone microenvironment by inhibiting calcium signaling which mediated early-stage bone colonization[11]. Arsenic trioxide was able to block multiple myeloma cells adhering to bone marrow stromal cells by inhibiting interleukin 6 and vascular endothelial growth factor secretion in the bone marrow microenvironment[12]. A low concentration of arsenic trioxide could inhibit osteoblast differentiation by reduction of runt-related transcription factor-2 (RUNX2) and osteocalcin expression in bone marrow stromal cells[13]. Arsenic trioxide also disturbed bone remodeling and reduced trabecular bone volume of the femur by decreasing osteoblast mineralization in rats[14]. However, arsenic trioxide is poisonous with cardiac toxicity, hepatotoxicity, renal failure, etc., depending on its exposure dosage *in vivo*. It also affected normal hematopoiesis in the bone marrow[15,16].

Here, arsenic trioxide was delivered specifically into the pre-metastatic osteogenic niches at the trabecular bone with immature HA. On one hand, the locally released arsenic would prevent the interactions of DTCs with neighboring osteoblast lineage cells and block their colonization in osteogenic niches. On the other hand, arsenic would inhibit the differentiation of osteoblast lineage cells from forming new bone and thus diminish the number of pre-metastatic niches available for bone colonization. Furthermore, the systemic toxicity of arsenic including bone marrow suppression would be minimized *in vivo*. In this study, we constructed an osteogenic niche-targeted polymeric nanocarrier to entrap arsenic-manganese (As-Mn) nanocrystals. DSS6 (DSSDSSDSSDS SDSSDSS) peptide was used as an osteogenic niche-targeting moiety. It could specifically bind to immature HAs at the endosteum of cancellous bone[17], where osteogenic niches always exist. We evaluated the effects of arsenic formulations on preventing tumor cell bone colonization *via* heterogeneous cell–cell adhesion, heterotypic organoid formation, and chemotactic migration in the mimic 3D osteogenic niche. We also tested the feasibility of delivering As-Mn nanocrystal containing nanoparticles into osteogenic niches for the treatment of breast cancer bone metastasis in the murine syngeneic bone metastasis model.

2. Materials and methods

2.1. Materials

Arsenic trioxide, Igepal CO-720, coumarin 6 and 3-(4,5-dimethylthiazol-2-yl)-2,5-diphenyltetrazolium bromide (MTT) were purchased from Sigma–Aldrich (St. Louis, MO, USA). Manganous acetate and chitosan were obtained from Macklin Biochemical Co., Ltd. (Shanghai, China). $MPEG_{5K}$-$PLGA_{20K}$ and $mPEG_{5K}$-PLA_{20K} were purchased from Yare Biotech, Inc. (Shanghai, China). Mal-PEG_{5K}-$PLGA_{20K}$ was synthesized in Hunan HuaTeng Co., Ltd. (Changsha, China). DSS6 (Ac-CDSSDSSDSSDSSDSSDSS) peptide was synthesized in Top-peptide Co., Ltd. (Shanghai, China). Hydroxyapatite (HA) was obtained from Emperor Nano Material Co., Ltd. (Nanjing, China). 1,1′-Dioctadecyl-3,3,3′,3′-tetramethylindotricarbocyanine iodide (DiR) was purchased from Meilun Biotech Co., Ltd. (Dalian, China). CellTracker Green 5-chloromethylfluorescein diacetate (CMFDA) was purchased from Yeasen Biotech Co., Ltd. (Shanghai, China). Puromycin dihydrochloride was purchased

from Beyotime Biotech Co., Ltd. (Shanghai, China). Anti-CD44-APC and anti-CD24-FITC were purchased from eBioscience (San Diego, CA, USA). MethoCult™ SF H4636 was purchased from STEMCELL Technologies Inc. (Vancouver, Canada).

2.2. Cell culture and animals

The murine mammary carcinoma cell line 4T1 was purchased from the Type Culture Collection of the Chinese Academy of Sciences (Shanghai, China). 4T1-RFP cell line was purchased from the AuLu Biotech Co., Ltd. (Shanghai, China). The murine embryonic mesenchymal stem cell (MSC) line C3H10T 1/2 and the murine preosteoblast cell line MC3T3-E1 were purchased from the Mingzhou Biotech Co., Ltd. (Ningbo, China). 4T1 with stable luciferase expression (4T1-luc) cell line was established by lentivirus infection. 4T1, C3H10T 1/2 and MC3T3-E1 cells were maintained in DMEM basic medium supplemented with 10% FBS, and 1% antibiotics (100 U/mL penicillin G and 0.1 mg/mL streptomycin). 4T1-RFP cells were maintained in DMEM medium supplemented with 10% FBS, 1% antibiotics, and puromycin dihydrochloride (3 μg/mL).

Female BALB/c mice (6−8 weeks, 18−20 g) were purchased from SLAC Laboratory Animal Co., Ltd. (Shanghai, China). All of the experiments were performed under experimental protocols approved by the Animal Care and Use Committee of Zhejiang Chinese Medical University, Hangzhou, China.

2.3. Methods

2.3.1. Preparation of As-Mn nanocrystal-loaded osteogenic niche-targeted nanoparticles

DSS6 peptide was conjugated with mal-PEG_{5K}-$PLGA_{20K}$ or mal-PEG_{5K}-PLA_{20K} by forming a thioether bond to obtain DSS6-PEG_{5K}-$PLGA_{20K}$ or DSS6-PEG_{5K}-PLA_{20K}. As-Mn nanocrystals were encapsulated in osteogenic niche-targeted nanoparticles *via* a modified double emulsion (w/o/w) method developed in our laboratory[18]. Briefly, 100 μL manganous acetate solution (65 mg/mL) was added in 1 mL dichloromethane solution with $mPEG_{5K}$-$PLGA_{20K}$/DSS6-PEG_{5K}-$PLGA_{20K}$ (1:1) or $mPEG_{5K}$-PLA_{20K}/DSS6-PEG_{5K}-PLA_{20K} (1:1, 20 mg/mL) and Igepal Co-720 (2.5 mg/mL) and sonicated to form w/o emulsion. Similarly, 100 μL arsenic trioxide solution (40 mg/mL, pH 8) was added in another dichloromethane solution with 1 mL polymer (20 mg/mL) and Igepal Co-720 (2.5 mg/mL) and sonicated to form another w/o emulsion. Both w/o emulsions were mixed gently and then added into 10 mL distilled water. The w/o/w double emulsion was formed *via* sonication for 2 min. The As^{3+} and Mn^{2+} were allowed to react in the inner water phase to form As-Mn nanocrystals. Dichloromethane was removed *via* rotary evaporation at 40 °C. The obtained nanoparticle suspension was further purified to remove the unentrapped arsenic. Coumarin 6/DiR-containing nanoparticles (0.05% *w/w*) were prepared *via* dissolving coumarin 6/DiR in dichloromethane with a similar method.

The drug loading content and entrapment efficiency were detected by an inductively coupled plasma-optical emission spectrometry (ICP-OES, ICAP-7400, Thermo Fisher, MA, USA). The size of nanoparticles was detected by a Nano-ZS90 ZetaSizer (Malvern Instruments, Worcestershire, UK), and their morphology was observed using a transmission electron microscope (TEM, H-7650, Hitachi, Tokyo, Japan). The size of As-Mn nanocrystals in nanoparticles was determined by Image J software (National Institute of Health, USA). The lyophilized nanoparticles were observed and their composition was detected by an energy dispersive X-ray spectrometry (EDX, AMETEK Materials Analysis Division, NJ, USA).

The arsenic released from osteogenic niche-targeted nanoparticles was detected by a dialysis method. 0.2 mL nanoparticle suspension was added in a dialysis bag (MWCO: 8−14 kDa) and placed into a centrifuge tube with 25 mL release medium (phosphate buffer saline, pH 5.0 or 7.4). It was then incubated in a shaker at 37 °C and 100 rpm (5810R, Eppendorf, Hamburg, Germany). 5 mL of release medium was withdrawn and an equal volume of fresh medium was added at predetermined time intervals. Arsenic concentration in the samples was detected by ICP-OES (Thermo Fisher).

2.3.2. In vitro and in vivo osteogenic niche targeting evaluation

The femurs were collected from sacrificed female BALB/c mice (6−8 weeks, 18−20 g). Bone marrow contents in femurs were flushed out or removed *via* sonication. The metaphyseal and diaphyseal bones were separated and dried in an oven at 80 °C. The bone fragments were finally obtained *via* pulverization. 1 mg metaphyseal or diaphyseal bone fragments were incubated with 0.2 mL coumarin 6-labeling untargeted or osteogenic niche-targeted nanoparticles (100 μg/mL) for 4, 12, or 24 h at 37 °C. After incubation, bone fragments were centrifuged and washed with PBS. Bone fragments with bound nanoparticles were imaged using an inverted microscope (EVOS FL, Thermo Fisher, MA, USA).

The targeting efficiency of the prepared nanoparticles into the osteogenic niche *in vivo* was evaluated as follows: 0.1 mL of DiR-labeling nanoparticles were injected intravenously into female BALB/c mice (6−8 weeks, 18−20 g). Mice were imaged at 2, 8, and 24 h with an IVIS® Lumina III Imaging System (PerkinElmer, USA). The main tissues of sacrificed mice were separated and imaged again at 24 h. The fluorescent images were acquired and fluorescence intensity in a specific area or each tissue was analyzed using Living Image Version 4.4 Software (PerkinElmer, USA).

2.3.3. Cell proliferation assay

4T1, C3H10T 1/2, or MC3T3-E1 cells were seeded in 96-well plates at a density of 5×10^3 cells/well and cultured overnight for cell attachment. The cells were then cultured with the medium containing a series of concentrations of arsenic formulations (0, 2.5, 5, 10, 15, and 20 μmol/L) for 72 h. MTT was added to each well and incubated for 4 h. The medium was then discarded and 200 μL DMSO was added into each well. Finally, the absorbance at 490 nm was detected by a microplate reader (Synergy H1, BIO TEK, Winooski, VT, USA).

2.3.4. Heterogeneous cell-cell adhesion assay

C3H10T 1/2 or MC3T3-E1 cells were incubated in 96 well plates for nearly 100% confluence and then were treated with arsenic formulations (5 or 10 μmol/L) for 24 h. After removing the drug-containing medium, 4T1-RFP cells (5000/well) in 200 μL Dulbecco's phosphate-buffered saline (DPBS) with calcium and magnesium were added into the wells allowing contact with pre-treated C3H10T 1/2 or MC3T3-E1 cells and incubated for 30 min at 4 °C. The non-adherent 4T1-RFP cells were removed. The adherent cells were visualized and counted under inverted fluorescence phase contrast microscope (Ti-S, Nikon, Tokyo, Japan).

2.3.5. Colony-forming unit (CFU) assays

C3H10T 1/2 or MC3T3-E1 cells in 6 well plates were treated with different arsenic formulations (5 or 10 μmol/L) for 24 h. Fresh medium was added into the wells and incubated for another 8 h after washing out of drug in each well. After 8 h incubation, a conditional medium from arsenic-treated MC3T3-E1 or C3H10T 1/2 cells was prepared. For CFU assay, 4T1 cells (2000/well) suspended in the mixture of Methocult H4236 medium and conditional medium (4:1) with 10% FBS were added in a 6 well plate (1 mL/well). The cell colonies in each well were imaged and counted after 3 days of incubation in a 37 °C and 5% CO_2 incubator.

2.3.6. Alkaline phosphatase (ALP) assay

MC3T3-E1 cells (2×10^4/well) were seeded in 6 well plates and cultured overnight for cell attachment. The cells were then treated with different arsenic formulations (5 μmol/L) for 24 h. After washing with PBS twice, cells were further cultured for 4 days and fixed for 10 min. The ALP levels were detected by BCIP/NBT Alkaline Phosphatase Color Development Kit (Beyotime Biotech Co., Ltd., Shanghai, China). The ALP staining with BCIP/NBT working solution was conducted in dark at 37 °C for 30 min. Cells were washed with distilled water twice and visualized using an inverted microscope (Leica DM i1, Leica Microsystems, Germany).

2.3.7. Osteogenic gene analysis

To measure gene expression by quantitative real-time reverse transcription polymerase chain reaction (RT-PCR), C3H10T 1/2 or MC3T3-E1 cells in 6 well plates (2×10^4/well) were treated with different arsenic formulations (5 μmol/L) for 24 h. Total RNA was extracted from treated MC3T3-E1 or C3H10T 1/2 cells with the Trizol reagent (Life Technologies). The following primer sequences were used for PCR reactions: *Runx2* (5′-CCCAGCCACCTTTACCTACA-3′, 3′-TATGGAGTGCTGCTGGTCTG-5′); *Osteopontin* (*Opn* (5′-TGATGATGACGATGGAGACC-3′, 3′-GGGACGATTGGAGTGAA AGT-5′); and *Osteocalcin* (*Ocn* (5′-GACCCTCTCTCTGCTCACTC-3′, 3′-CACCTTACTGCCCTCCTGC-5′). The mRNA levels were normalized to *β*-actin (5′-AGCCTTCCTTCTTGGGTATG-3′, 3′-GGTCTTTACGGATGTCAACG-5′) and relative gene expression was calculated using the $2^{-\Delta\Delta Ct}$ method.

2.3.8. Co-culture of 4T1 cells with MSCs or osteoblastic cells

CellTracker Green CMFDA-labeling C3H10T 1/2 or MC3T3-E1 cells following the manufacturer's instructions were treated with different arsenic formulations (5 or 10 μmol/L) for 24 h. After removing the medium, pretreated C3H10T 1/2 or MC3T3-E1 cells were seeded into 96 well ultra-low attachment plates (20,000 cells/well) and cultured with untreated 4T1-RFP cells (10,000 cells/well). The heterotypic organoids were grown for 4 days. The morphology and fluorescence image of organoids were captured with inverted fluorescence phase contrast microscope (Nikon). The sizes of organoids were determined by Image J software (National Institutes of Health).

2.3.9. Flow cytometry analysis of $CD44^+CD24^-$ subpopulation in 4T1-RFP cells of heterotypic organoids

MC3T3-E1 cells were treated with different arsenic formulations (5 μmol/L) for 24 h 4T1-RFP and pretreated MC3T3-E1 cells (1:2) were resuspended in DMEM and then mixed at a total cell concentration of 3×10^4 cells/mL. Heterotypic organoids were obtained after co-culture for 3 days. The single cell suspension was obtained by digesting each organoid with trypsin. Cells were washed and incubated with CD44-APC and CD24-FITC antibodies at 4 °C in dark for 15 min. The $CD44^+$ $CD24^-$ subpopulation in 4T1-RFP cells of heterotypic organoids was determined using a flow cytometry (LSR Fortessa, BD, NJ, USA).

2.3.10. Cell migration in mimic 3D osteogenic niche in vitro

3D osteogenic niche was mimicked and prepared with 3D porous chitosan scaffold containing porous nanostructure and osteogenic cells *in vitro*. 3D porous chitosan scaffold containing 10% (*w*/*w*) HA was fabricated *via* lyophilization following a previously reported protocol with modifications[19]. Briefly, 0.45 g chitosan (96% deacetylated) was added to 50 mL 2% acetic acid and stirred for 1 h for complete dissolution. Meanwhile, 10% (*w*/*w*) HA was added and sonicated for 10 min. The HA/chitosan solution was poured into a silicone mold and then frozen at −80 °C. The frozen samples were lyophilized and then imaged by a scanning electron microscope (SEM, SU8010, Hitachi, Tokyo, Japan).

The lyophilized scaffold samples were rinsed with 1 mol/L NaOH to neutralize the residual acetic acid. MC3T3-E1 cells were pretreated with the arsenic solution (10 μmol/L) for 12 h. Pretreated MC3T3-E1 cells (20,000) were washed and seeded into the scaffolds. 4T1-RFP cells (30,000) pretreated with the arsenic solution (4 μmol/L) for 12 h were washed and co-seeded. The images of the entire scaffolds were captured by an inverted confocal microscope (LSM880, Carl Zeiss AG, Jena, Germany) after culture for 3 days. To visualize the migration depth and distribution of 4T1-RFP cells in the mimic 3D osteogenic niche, series of Z-stack images for each tile were acquired and reconstructed to show 3D images.

2.3.11. Evaluation of therapeutic efficacy in vivo

To establish murine bone metastasis model, female BALB/c mice (6−8 weeks, 18−20 g) were inoculated with 5×10^4 4T1-luc cells *via* intracardiac route into the left ventricle. The mice were randomly divided into 5 groups: (1) control (ctrl), (2) arsenic solution (free As), (3) arsenic-loaded nanoparticle (As NP), (4) As-Mn-loaded nanoparticle (untargeted), (5) osteogenic niche-targeted As-Mn-loaded nanoparticle (targeted). Arsenic was administered (2 mg/kg) *via* tail vein twice per week for a total of 5 times from the day before 4T1-luc cell inoculation. Tumor growth was monitored weekly *via in vivo* bioluminescence imaging. Body weight was measured twice per week. Mice were monitored daily, and animals were sacrificed at signs of morbidity. To evaluate 4T1 tumor bone metastasis, mice with 4T1-luc cells by intracardiac inoculation received the same treatments as described above, and were sacrificed 2 weeks later. Spine and femur samples were collected, fixed, and decalcified with formic acid decalcification solution. Tissue blocks were processed for H&E staining.

2.3.12. In vivo toxicity evaluation

Female BALB/c mice (6−8 weeks, 18−20 g) were administrated with (1) control, (2) free As (2 mg/kg), (3) As NP (2 mg/kg), (4) untargeted (2 mg/kg), (5) targeted (2 mg/kg) *via* tail vein injection twice per week for 5 times. Body weight was measured twice per week. Blood samples were collected for hematology analysis 24 h after the last treatment. Alanine aminotransferase (ALT), aspartate aminotransferase (AST), blood urea nitrogen (BUN), and creatinine (CREA) in serum samples were measured. The major tissues including the spine and femurs were collected, sectioned, and stained with hematoxylin and eosin (H&E) for histological analysis.

2.3.13. Statistical analysis

All *in vitro* and *in vivo* experiments were performed at least three times and the data are presented as means ± SD, if not indicated differently. Student's *t*-test was used to compare the differences in groups unless otherwise indicated. $P < 0.05$ was considered significant.

3. Results

3.1. Characterization of osteogenic niche-targeted As-Mn nanocrystal containing nanoparticles

We have developed a facile modified double emulsion (w/o/w) method to entrap As-Ni transitional metal compounds as nanocrystals into biocompatible polymeric nanoparticles using the Igepal series of surfactants for the first time in our previous study[18]. The arsenic loading content and stability in polymeric nanocarriers have been remarkably improved. Recently, it was demonstrated that Mn(II) ion-containing nanoparticles with 7−25 nm had high T1 relaxivity as Mn-based magnetic resonance imaging contrast agents for clinical application[20]. Here, we further tested the feasibility of encapsulation of As-Mn nanocrystals in polymeric nanoparticles. TEM images showed that As-Mn nanocrystals were successfully entrapped in PEG_{5k}-$PLGA_{20k}$ and PEG_{5k}-PLA_{20k} nanoparticles with Igepal Co-720 as a surfactant (Fig. 1A and Supporting Information Fig. S1A). The average size of As-Mn nanocrystals depositing in nanoparticles was 14 nm with a narrow distribution. Arsenic loading content in PEG-PLGA nanoparticles with As-Mn reached 4.75%, which was significantly higher than that with arsenic alone (1.29%). The size and zeta potential of As-Mn nanocrystal-loaded PEG_{5k}-$PLGA_{20k}$ nanoparticles were relatively stable compared with that of PEG_{5k}-PLA_{20k} nanoparticles in a high concentration of serum (Fig. S1B). Therefore, we chose PEG_{5k}-$PLGA_{20k}$ as the polymeric carrier. EDX elemental mapping demonstrated that there were ample manganese and arsenic atoms in the polymeric nanoparticles (Fig. 1B and C).

It was reported that an acidic microenvironment triggered the dissociation of As-Mn complexes[21]. We detected the release of arsenic from As-Mn nanocrystal-loaded nanoparticles at pH 7.4 and 5.0 (Fig. 1D and Fig. S1C). There was relatively low arsenic release (less than 25%) from PEG-PLGA and PEG-PLA nanoparticles at pH 7.4, demonstrating the relatively stable arsenic entrapment in blood circulation. However, the cumulative arsenic release quickly increased at 1 h in pH 5.0 release medium. It reached 68.2% and 74.4% from As-Mn-loaded PEG-PLGA and PEG-PLA nanoparticles, respectively. The low pH-induced dissociation of As-Mn nanocrystals could cause the formation of nanopores in polymeric nanoparticles and thus accelerate the degradation of copolymers in an acidic release medium. The results suggested that arsenic was easily released from As-Mn nanocrystal containing nanoparticles in the acidic endosome/lysosome microenvironment once they were internalized in the targeted cells.

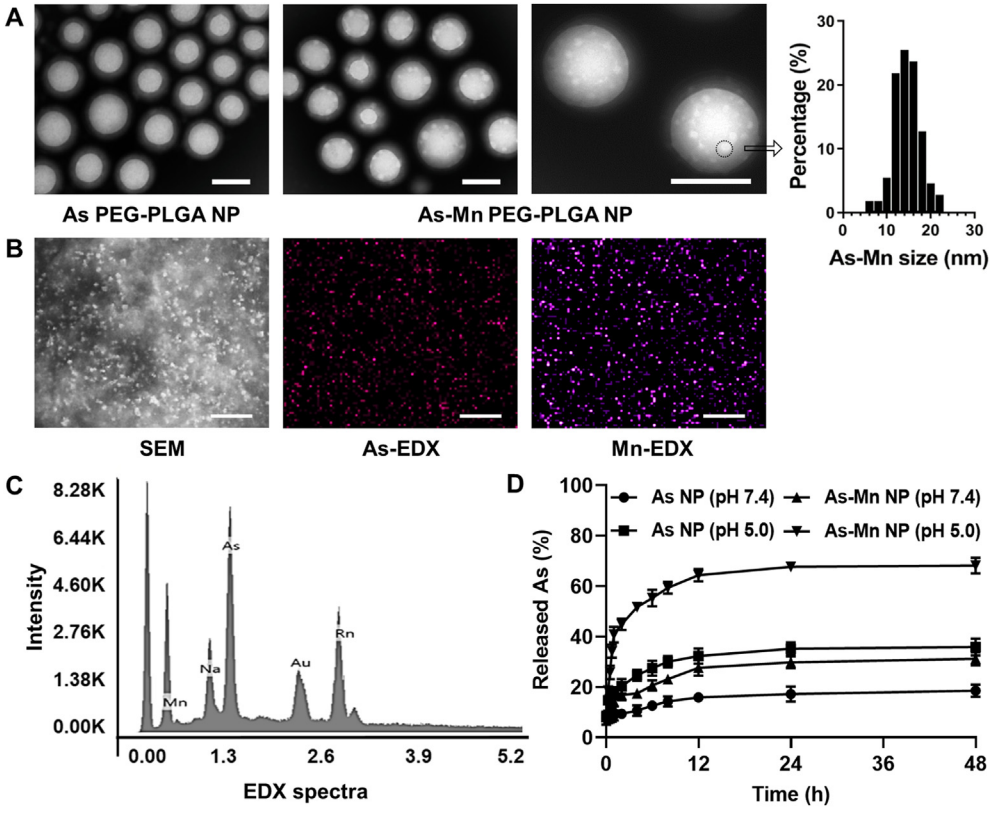

Figure 1 Characterization of As-Mn nanocrystal-loaded PEG_{5k}-$PLGA_{20k}$ nanoparticles. (A) Morphology of As-Mn-loaded nanoparticles and size distribution of As-Mn nanocrystals inside nanoparticles. TEM scale bar = 200 nm. (B) SEM image and EDX mapping of As-Mn-loaded nanoparticles. Scale bar = 20 μm. (C) EDX Spectra of As-Mn-loaded nanoparticles. (D) Arsenic release from PEG_{5k}-$PLGA_{20k}$ nanoparticles in pH 7.4 and 5.0 release media. As NP, arsenic-loaded nanoparticle; As-Mn NP, As-Mn-loaded nanoparticle ($n = 3$).

3.2. *The osteogenic niche targeting efficiency*

The osteogenic niches were always located at the endosteum of cancellous bone with immature HA[8,9]. DSS6 peptide showed a specific binding capability to immature HA with amorphous calcium phosphate crystals[22]. Our previous results demonstrated that 50% of DSS6 conjugation could guide the nanoparticles to preferentially bind to metaphyseal bone fragments, representing immature HAs *in vitro*[18]. The fluorescence in metaphyseal bone, which was treated with coumarin 6-labeling untargeted nanoparticles, was relatively weaker than that of osteogenic niche-targeted nanoparticles and showed no change with the increase of incubation time (Fig. 2A). However, the quantitative fluorescence intensity in metaphyseal bone treated with targeted nanoparticles was 2.1-fold compared with untargeted nanoparticles at 24 h (Fig. 2B). Both targeted and untargeted nanoparticles treated diaphyseal bone fragments representing the well-oriented HAs showed similar fluorescence intensity at each time point (Supporting Information Fig. S2).

The osteogenic niche targeting efficiency *in vivo* was evaluated *via* intravenous injection of DiR-labeling nanoparticles in BALB/c mice. The fluorescence intensity and distribution in the whole mice were approximate at 2 h after tail vein injection (Fig. 2C). Notably, there were significant differences between the two treatment groups at 8 and 24 h. It showed obvious fluorescence in skull, spine, and femoral trabecular bone in the targeted treatment group. The cumulative total radiant efficiency of skull, spine, and femoral trabecular bone in targeted nanoparticle-treated mice increased 3.4 and 5.1 times compared with that of untargeted nanoparticle-treated mice at 8 and 24 h, respectively (Fig. 2D). The *ex vivo* main tissue images demonstrated DSS6 peptide-modified nanoparticles could enrich DiR in the spine and leg, especially in the trabecular bone of the femur and tibia (Fig. 2E). The fluorescence signals in the other tissues were close in both treatment groups. The DiR content of targeted nanoparticles was increased 2.2- and 2.7-fold than that of untargeted nanoparticles in the spine and leg, respectively (Fig. 2F). The above results suggest that targeted nanoparticles had the capability of selective binding

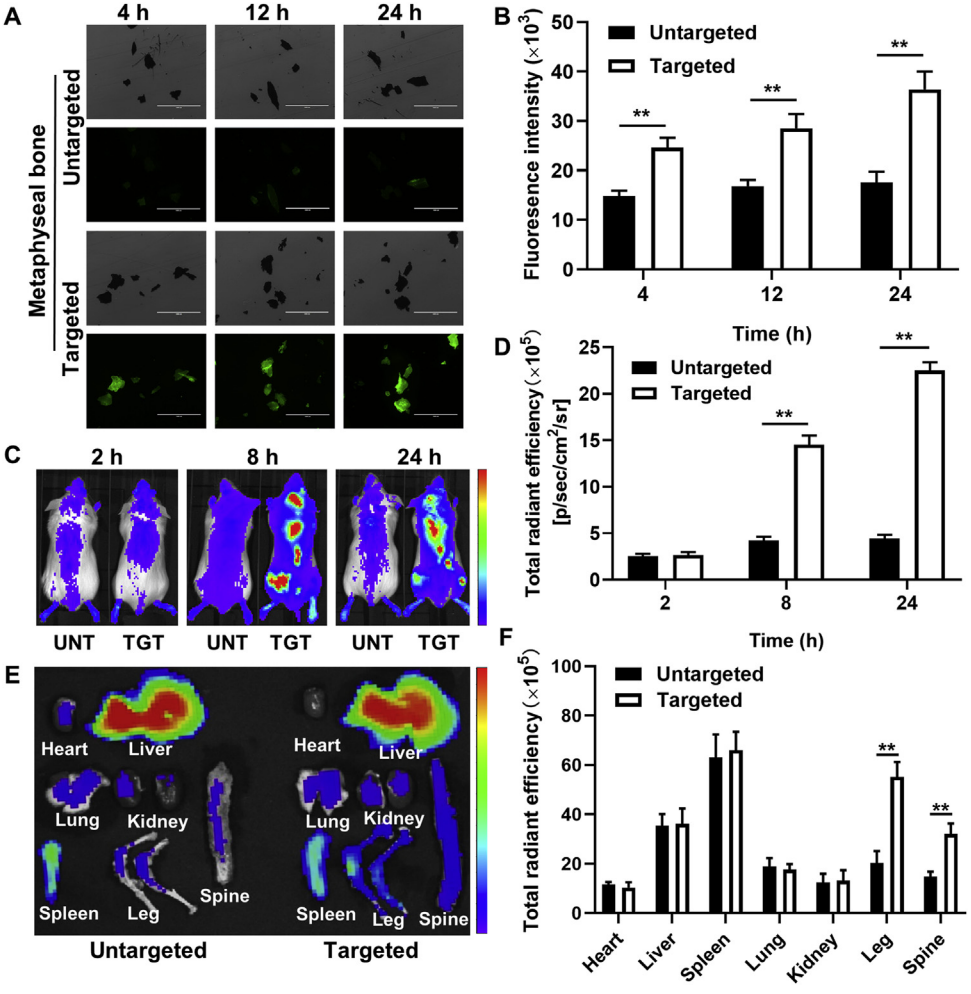

Figure 2 The osteogenic niche binding capability of 50% DSS6 conjugated nanoparticles. (A) Coumarin 6-labeling untargeted or targeted nanoparticles binding with metaphyseal bone fragments for different time intervals. Scale bar = 1 mm. (B) Green fluorescent intensities with different incubation time ($n = 3$). (C) Fluorescence images of whole mouse body after intravenous injection of DiR-labeling nanoparticles for 2, 8, and 24 h (UNT, untargeted; TGT, targeted). (D) Total quantitative fluorescence intensities of skull, spine, and hind legs in untargeted and targeted groups at 2, 8, and 24 h. (E) Fluorescence images of dissected major tissues in mice after treated with DiR-labeling nanoparticles for 24 h. (F) Fluorescence quantification of major tissues in mice injected with DiR-labeling nanoparticles for 24 h ($n = 4$). Data are presented as mean ± SD. $^{**}P < 0.01$.

to the trabecular bone both *in vitro* and *in vivo*, where the osteogenic niches always existed.

3.3. *Arsenic inhibits tumor cell adhesion and osteogenic differentiation in the osteogenic niche*

In the initial stage of bone metastasis, DTCs enter the bone marrow and colonize into the bone microenvironment. The osteogenic niches have been found to determine the DTC fate[5]. To investigate the effects of arsenic in regulating tumor cell colonization in breast cancer bone metastasis, we evaluated *in vitro* heterogeneous cell-cell adhesion, and 4T1 colony formation in the C3H10T 1/2 or MC3T3-E1 cell mimic bone microenvironment. The results revealed that 4T1-RFP cells could heterogeneously adhere to C3H10T 1/2 or MC3T3-E1 cells (Fig. 3A). The IC_{50} of arsenic were 4.7, 17.6, and 15.9 μmol/L in 4T1, C3H10 1/2, and

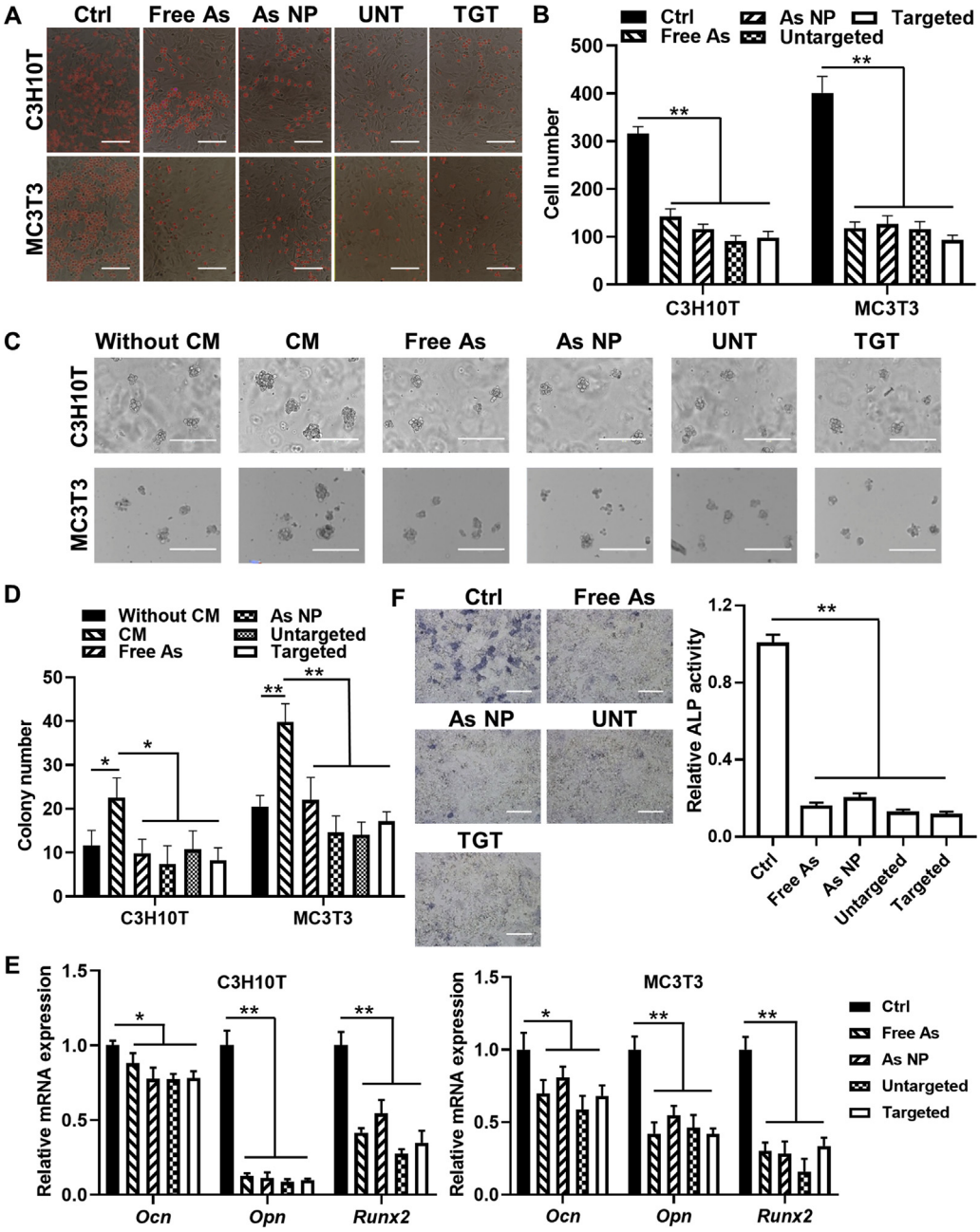

Figure 3 Arsenic formulations inhibit tumor cell adhesion and osteogenic differentiation in the osteogenic niche microenvironment. (A) Adhesion of untreated 4T1-RFP cells to C3H10T 1/2 or MC3T3-E1 cells pretreated with different arsenic formulations at 5 μmol/L for 24 h (scale bar = 100 μm), and (B) cell number analysis of adhesive 4T1-RFP cells. (C) Representative 4T1-RFP cell colonies in the conditional medium (CM) from C3H10T 1/2 or MC3T3-E1 cells pretreated with arsenic formulations at 5 μmol/L for 24 h (scale bar = 100 μm), and (D) the statistical analysis of 4T1-RFP cell colony numbers. (E) The relative gene expression of *OCN*, *OPN*, and *Runx2* in C3H10T 1/2 or MC3T3-E1 cells treated with arsenic formulations at 5 μmol/L for 24 h. (F) Images of alkaline phosphatase (ALP) staining (scale bar = 100 μm) and the relative ALP activity of MC3T3-E1 cells on Day 4 after treatment with arsenic formulations at 5 μmol/L for 24 h. Data are presented as mean ± SD. ($n = 3$, $^{*}P < 0.05$, $^{**}P < 0.01$).

MC3T3-E1 cells for a 72 h exposure, respectively (Supporting Information Fig. S3A). When C3H10T 1/2 or MC3T3-E1 cells were pretreated with arsenic formulations at 5 μmol/L for 24 h, 4T1 cells adhered to C3H10T 1/2 or MC3T3-E1 cells diminished at least 55% and 68%, respectively (Fig. 3B). 4T1 cells adhered to pretreated MSCs or osteogenic cells at 10 μmol/L were less than 13% of the corresponding untreated group (Fig. S3B). These results indicated that arsenic pretreatment blocked the seeding of tumor cells in the osteogenic niches.

After seeding, the next step for tumor cells is to adapt to the microenvironment of osteogenic niches. Therefore, we detected the dependent growth in Methocult medium with conditioned medium from C3H10T 1/2 or MC3T3-E1 cells. It was observed that the conditioned medium significantly promoted the proliferation of 4T1 cells with bigger colony sizes and more numbers than that of the normal medium. On the other hand, the sizes and numbers of 4T1 cell colonies *via* culture in conditioned medium from pretreated osteogenic cells with arsenic formulations (5 or 10 μmol/L) were restored to that in normal medium (Fig. 3C and D, and Fig. S3C and D).

The interactions between tumor cells and MSCs/osteogenic cells were usually regulated by the locally produced soluble factors such as chemokines and growth factors[23]. The results of RT-PCR analysis showed that the expression of *Runx2* and *Opn* genes in C3H10T 1/2 or MC3T3-E1 cells treated with arsenic formulations (5 μmol/L) was significantly decreased, while *OCN* expression was slightly decreased compared with the control group (Fig. 3E). Down-regulation of *Runx2* could reduce the expression of vascular endothelial growth factor (VEGF) and matrix metalloproteinase and further inhibit bone colonization[24]. *Opn* mediated the interaction of $\alpha_v\beta_3$-integrin of tumor cells with osteogenic cells[25]. Decreased *Opn* expression prevented the tumor cell adhesion in the bone microenvironment.

The metastatic osteogenic niches were found in the metaphyseal trabecular bone with high bone anabolic activity in mice[7]. A mammary tumor remotely altered metaphyseal bone mineral by decreasing the local HA crystallinity[8]. The ALP activity is the most widely recognized biochemical marker for bone anabolic activity[26]. We found that arsenic treatment at 5 μmol/L for 24 h reduced the ALP activity by around 85% compared with that of control in MC3T3-E1 cells on Day 4 (Fig. 3F). Importantly, *Runx2* is an essential transcription factor for osteogenic differentiation, driving the stage-transition of osteoblast phenotype and thereby serving a determinant function in bone formation[27]. *Opn*also participates in the regulation of the growth of HA crystals[28]. Therefore, arsenic formulations were able to reduce the number of pre-metastatic osteogenic niches available for bone colonization of tumor cells *via* inhibiting osteogenic differentiation and decreasing bone mineralization.

3.4. *Co-culture of breast tumor cells with osteogenic niche cells*

We conducted a co-culture of 4T1-RFP cells with Green Celltracker-labeling C3H10T 1/2 or MC3T3-E1 cells in 3D suspension conditions. 4T1 cells interacted with C3H10T 1/2 or MC3T3-E1 cells and formed a heterotypic spherical organoid with a shell of tumor cells and a core of osteogenic cells, which recapitulated the direct interaction between two kinds of cells. There was a clear boundary between the organoid and the culture medium in the control group. However, lots of cells scattered around the organoids when osteogenic niche cells were pretreated with arsenic formulations (5 or 10 μmol/L) (Fig. 4A and B, and Supporting Information Fig. S4A and B). Interestingly, these scattered cells were identified as 4T1-RFP cells with red fluorescence, which were not involved in the organoid formation. Meanwhile, arsenic pretreatment also shrank the sizes of heterotypic organoids (Fig. 4C). These results suggest that arsenic could alter the direct interaction between tumor cells and osteogenic niche cells, and then slowed the breast cancer cell colonization.

Breast tumor cells would survive and enter dormancy after bone colonization. Metastasis-initiating cells have many characteristics of cancer stem cells (CSCs) during dormancy[29]. Here, we tested the number of CSCs using $CD44^+CD24^-$ markers in the heterotypic organoids of breast tumor cells and osteogenic cells. The flow cytometry gating strategy used to study $CD44^+CD24^-$ 4T1-RFP cells are shown in Fig. S4C. 4T1-RFP cells only contained 0.14% $CD44^+CD24^-$ cells under a normal culture condition. The proportion of $CD44^+CD24^-$ cells surged to 21.2% in the 4T1-RFP-MC3T3-E1 organoids. However, CSCs decreased to around 7% when MC3T3-E1 cells were pretreated with arsenic formulations (5 μmol/L) (Fig. 4D and E). Given these results, arsenic pretreatment diminished the probability of colonized tumor cell dormancy in the osteogenic niches.

3.5. *Tumor cell migration in mimic 3D osteogenic niche in vitro*

To create a bone colonization model that contains the supportive porous nanostructure and to simulate the chemotactic migration process, MC3T3-E1 and 4T1-RFP cells were co-seeded into the scaffolds to mimic the spatial pre-metastatic osteogenic niche *in vitro*. The overall schematic illustration of the scaffold fabrication is shown in Fig. 5A. There were two types of cell behaviors inside the scaffold. The upper SEM image showed that the single cells adhered to the pores of the scaffold and could migrate (Fig. 5B). The bottom SEM image suggested that the cells colonized the pores and proliferated to cell aggregates. Both represented two different tumor cell behaviors in the bone marrow microenvironment.

To visualize the tumor cell migration depth and distribution in the predetermined time, 3D cell images were constructed by Z-stack scanning images of the entire scaffold thickness (Fig. 5C). The migration depth of 4T1-RFP cells in the scaffold was 5180 μm, in which both 4T1-RFP and MC3T3-E1 cells were untreated. In contrast, the migration depth of 4T1-RFP cells was only 2400 μm, in which both 4T1-RFP and MC3T3-E1 cells were pretreated with arsenic at 4 and 10 μmol/L for 12 h before seeding into the scaffold, respectively. Fig. 5D shows the cross-section of both scaffolds at the depth of 3000 μm in both scaffolds. It indicated that there was much stronger red fluorescence of 4T1-RFP cells in the untreated scaffold compared with that treated with arsenic. These results reveal that the chemotactic migration of 4T1-RFP cells toward MC3T3-E1 cells could be blocked *via* arsenic treatment in the mimic spatial osteogenic niche.

3.6. *Therapeutic efficacy of arsenic formulations on breast tumor bone metastasis*

The BALB/c syngeneic breast tumor bone metastasis model was developed by intracardiac inoculation of 5×10^4 4T1-luc cells. We treated mice bearing 4T1 bone metastasis with different arsenic formulations twice weekly and monitored the disease progression (Fig. 6A). The results show that the mice in the untreated group had obvious bone metastases, and the bioluminescence was distributed in the mouse skull, spine, and hind leg on

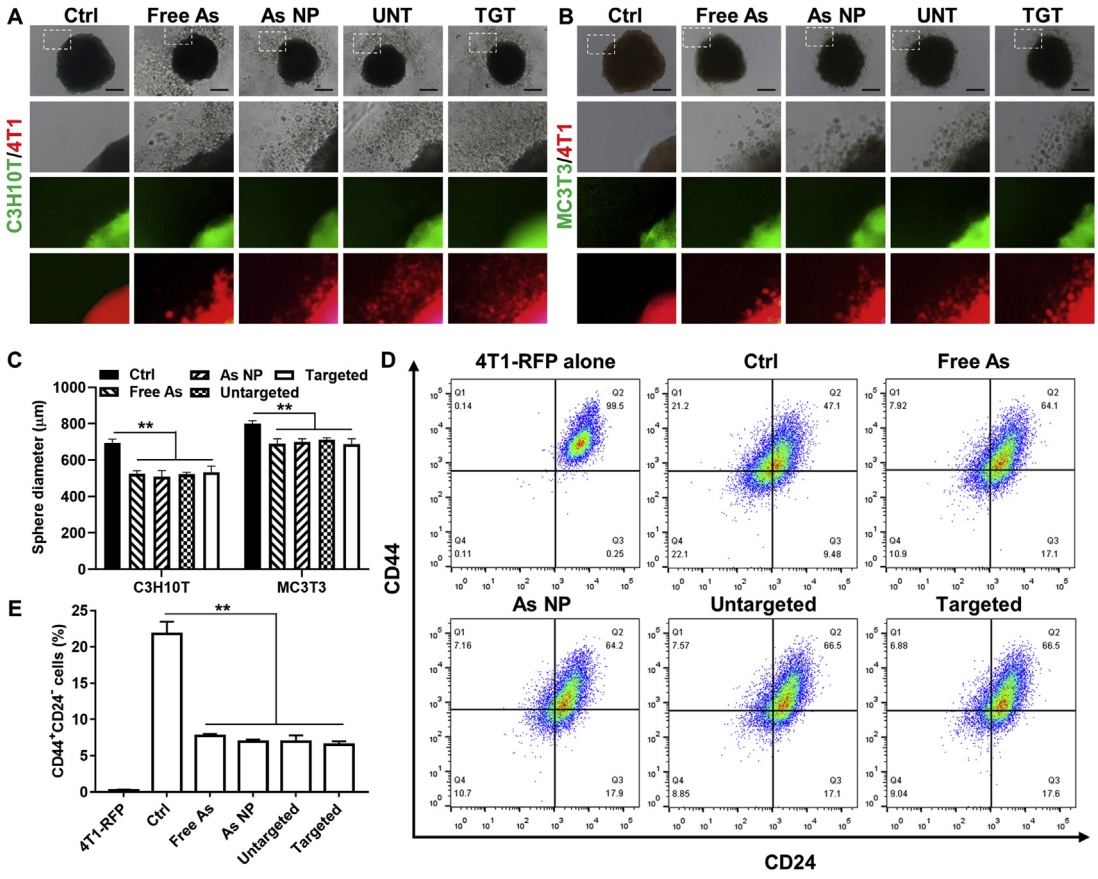

Figure 4 Arsenic formulations prevent the direct contact of tumor cells with osteogenic cells and the dormancy of tumor cells in heterotypic organoids. Bright-field and fluorescence images of organoids formed by untreated 4T1-RFP cells and pretreated CMFDA-labeled C3H10T 1/2 cells (A) or MC3T3-E1 cells (B) with arsenic formulations at 5 μmol/L for 24 h (lines 2−4 show corresponding magnification images of dotted rectangular regions in line 1, green: C3H10T 1/2 or MC3T3-E1 cells, red: 4T1-RFP cells, scale bar = 200 μm), and the statistical analysis of their sizes (C). Representative flow cytometry images (D) and the statistical analysis (E) of $CD44^{+}CD24^{-}$ subpopulation of 4T1-RFP cells in heterotypic organoids of 4T1-RFP and MC3T3-E1 cells, in which MC3T3-E1 cells were pretreated with arsenic formulations at 5 μmol/L for 24 h. Data are presented as mean ± SD ($n = 3$, $^{**}P < 0.01$).

Day 7 after inoculation (Fig. 6B). Bone metastasis occurred in mice treated with free As and As NPs, but bone metastasis only occurred in one mouse treated with targeted NPs on Day 7. The degree of bone metastasis in mice after administration of targeted NPs was significantly retarded, and its bioluminescence was significantly lower than the other treatment groups on Day 14 (Fig. 6C).

The syngeneic 4T1-luc breast tumor cells grew very aggressively inside the mouse body. All untreated mice died from bone metastasis Days 11−17 after cell inoculation (Fig. 6D). There was no survival benefit from treatment with free As and As NPs. Their median survival times were 17 and 17.5 days, respectively. In contrast, significant therapeutic efficacy was achieved in mice treated with untargeted and targeted NPs, with median survival times of 19 and 23 days, respectively. The best therapeutic outcome was from mice treated with targeted NPs. Meanwhile, mice with bone metastasis experienced great loss of body weight during the late stage in the control, free As and As NP groups (Fig. 6E). The body weight loss was alleviated in the untargeted and targeted NP treatment groups. Furthermore, the mice were sacrificed and their spine and femur samples were collected for histologic analysis on Day 14 (Fig. 6F). The bone metastatic tumor cells were mainly located in the trabecular bone below the growth plate cartilage of the femur and the vertebral body of the spine, where the osteogenic niches always existed. This observation was histologically similar to those obtained in the published studies[7,8]. Breast tumor nodules in the femur and spine of the targeted NP treatment group were significantly smaller compared with those in the other treatment groups.

3.7. *In vivo toxicity of arsenic formulations*

The toxicity of arsenic trioxide depends on its exposure dosage *in vivo*. Its toxic symptoms mainly include cardiac failure, renal failure, flaccid paralysis, etc.[30]. Therefore, we conducted *in vivo* studies to investigate the systemic toxicity of different arsenic formulations. The treatment regimen was the same as that in the therapeutic efficacy study. These mice were sacrificed 24 h after the last administration. Whole blood and serum samples were collected for analyzing the hematological and biochemical parameters. The numbers of red blood cells, platelets, and lymphocytes in the blood of mice with free As treatment decreased significantly, which suggested that intravenous injection of arsenic solution disturbed normal hematopoiesis in the bone marrow (Fig. 7A and B). In contrast, there was no bone marrow toxicity observed in the targeted nanoparticle treatment group. The levels

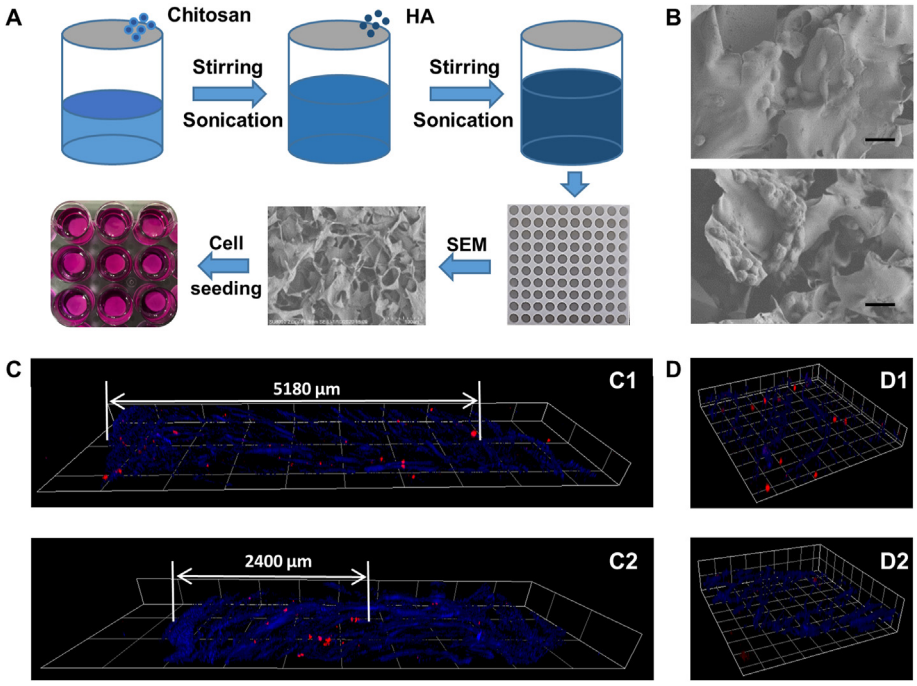

Figure 5 Arsenic trioxide inhibits tumor cell migration in mimic 3D osteogenic niche *in vitro*. (A) Schematic illustration of *in vitro* mimic 3D osteogenic niche fabrication. (B) SEM images of mimic 3D osteogenic niche with 4T1-RFP and MC3T3-E1 cells. Scale bar = 10 μm. (C) 3D reconstruction of longitudinal-section confocal microscopy images of 4T1-RFP cells (red) in chitosan/HA scaffold (blue) after culture for 3 days. 4T1-RFP and MC3T3-E1 cells were untreated (C1, 1 unit = 700 μm). 4T1-RFP and MC3T3-E1 cells were pretreated with arsenic at 4 and 10 μmol/L for 12 h, respectively (C2, 1 unit = 600 μm). (D) 3D reconstruction of cross-section images of 4T1-RFP cells (red) in chitosan/HA scaffold (blue) after culture for 3 days. 4T1-RFP and MC3T3-E1 cells were untreated (D1). 4T1-RFP and MC3T3-E1 cells were pretreated with arsenic at 4 and 10 μmol/L for 12 h, respectively (D2). 1 unit = 100 μm.

of ALT and AST used for liver function analysis were elevated in free As and untargeted nanoparticle treatment group (Fig. 7C). However, there was no change of ALT and AST values in the targeted NP treatment groups. There was remarkable body loss in the free As and As NP treatment groups on Days 14 and 18 compared to that in the control group (Fig. 7D). The body weights were similar in the control, untargeted, and targeted nanoparticle treatment groups. No obvious morphological abnormalities were observed based on H&E staining in the histological analysis (Fig. 7E and Supporting Information Fig. S5). These results demonstrate that the osteogenic niche-targeted nanoparticles reduced the bone marrow and hepatic toxicity of arsenic in normal mice.

4. Discussion

Bone metastasis frequently occurs in advanced breast cancer patients, causing significant morbidity. The current treatment approaches used in the clinic are largely palliative. These strategies usually tried to minimize the overt tumor nodules or improve the life quality of patients in the late manifestation of the clinical metastasis stage[31]. There is an urgent need to develop additional therapies. Here, we showed that arsenic formulation blocked tumor cell colonization in the bone microenvironment, indicating the importance of preventing bone colonization in the treatment of metastasis. Our study may lay the groundwork for novel and more effective therapeutic concepts in the early stages of the metastatic process.

Disseminating tumor cells preferentially metastasize to bone determined by their dynamic interactions with the bone marrow and mineralized bone matrix. Specific chemokines and cell adhesion initiate tumor cell colonization in the bone microenvironment[32]. It is well recognized that bone resident cells, especially osteoblastic lineage cells, promote cancer cell seeding and growth in the pre-metastatic osteogenic niche[5]. Osteoblastic lineage cells comprise cells of different differentiation stages from MSCs to osteoprogenitors, osteoblasts, and ultimately cortical lining cells or osteocytes[33]. They not only directly secreted chemokines and meditated cell adhesion *via* gap junctions, but also produced predominantly structural proteins to construct the pre-metastatic niche[34]. In this context, we showed that both conditional media from MSCs and osteobastic cells promoted the colony formation of cancer cells. Importantly, MSCs/osteobastic cells could induced cancer cell dormancy *via* direct contact through greatly increasing the $CD44^{+}CD24^{-}$ subpopulation of breast cancer cells, representing cancer stem cells.

Numerous studies have focused on elucidating the complex cellular and molecular mechanisms within the bone marrow that are responsible for tumor cell colonization and dormancy[35]. However, there is no effective therapeutic strategy against bone colonization in the initial stage of bone metastasis. Our results indicated that arsenic prevented the adhesion of tumor cells to osteogenic cells and inhibit their proliferation in conditional medium from cultured osteogenic cells. Arsenic also hampered the direct interaction between 4T1 cells and osteogenic cells, especially diminished the ratio of dormant cancer stem cells in heterotypic organoids. The chemotactic migration of tumor cells

toward osteogenic cells was slowed in the mimic 3D osteogenic niche. Thus, arsenic could prevent the colonization of disseminated breast tumor cells in the osteogenic niche *in vitro*.

How to specifically deliver arsenic into pre-metastatic osteogenic niches *in vivo*? Devignes et al.[7] observed that early breast cancer cells colonized specific bone microenvironment particularly enriched in osteoprogenitors. Disseminated tumor cells were never found in epiphysis bone that has fewer or no osteoprogenitor. This bone microenvironment was located in trabecular bones next to the growth plate cartilage in mice. Preferential metastatic localization in human was observed in the trabecular bone-rich pelvis and spinal vertebral bodies in the clinic[9]. Previous reports further showed that these trabecular bones were always composed of immature HA crystals with a decreased

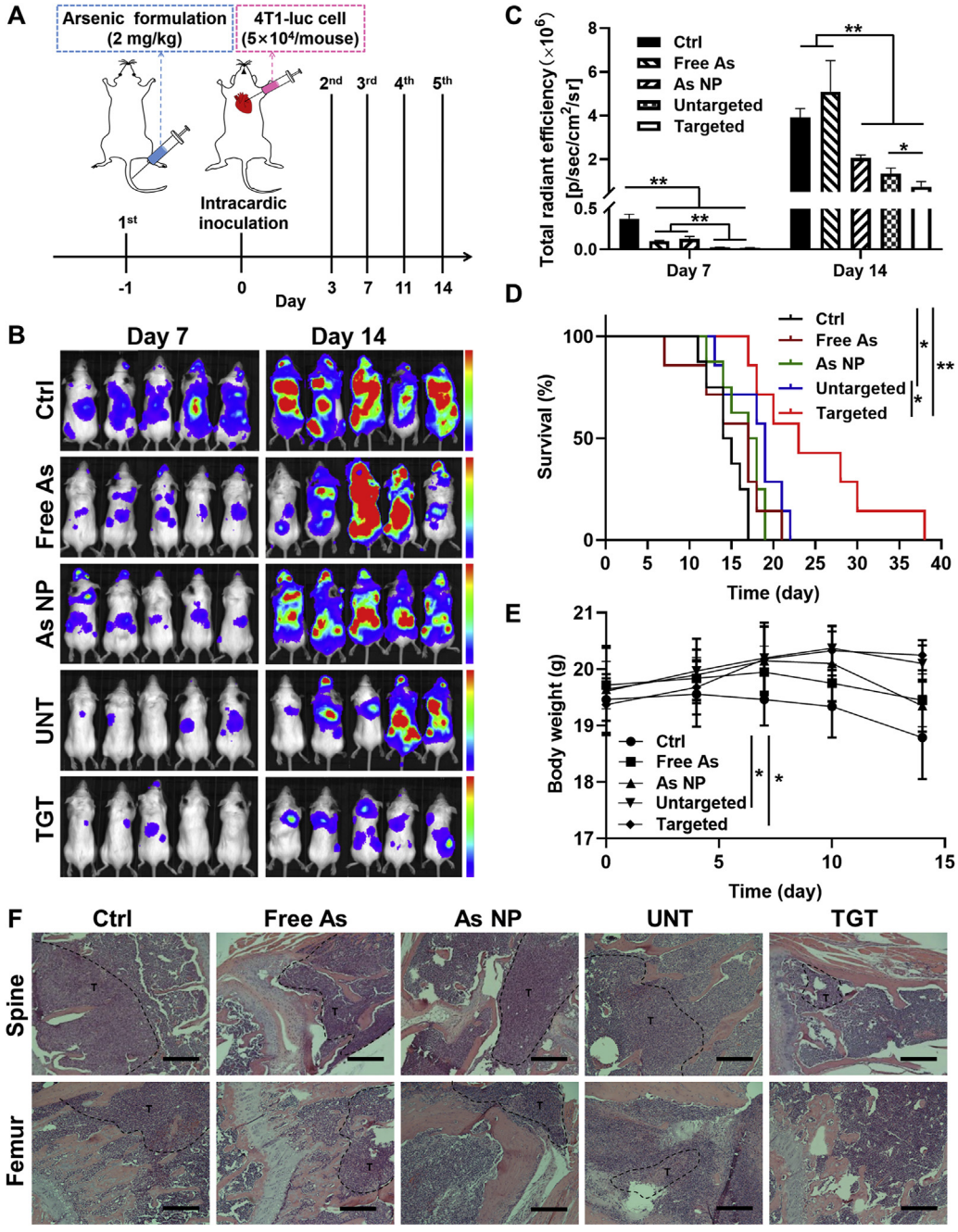

Figure 6 *In vivo* therapeutic efficacy of arsenic formulations in 4T1 syngeneic bone metastasis model (ctrl, $n = 8$; free As, $n = 7$; As NP, $n = 8$; untargeted, $n = 7$; targeted, $n = 7$). (A) Experimental timeline for the therapeutic efficacy study. (B) Representative bioluminescence images of mice bearing 4T1 metastatic tumors treated with different arsenic formulations. (C) Tumor burden measured by *in vivo* bioluminescence imaging (mean ± SEM). (D) Kaplan−Meier plot on animal survival in mice bearing 4T1 metastatic tumors treated with different arsenic formulations, log-rank (Mantel−Cox) test is used to compare the differences. (E) Average body weights of mice treated with different arsenic formulations (mean ± SD; *, for comparisons of indicated groups on Days 10 and 14). (F) H&E staining of the spine and femur of 4T1 metastatic tumor-bearing mice in each treatment group. The dotted line area shows the dense tumor cells. Scale bars = 500 μm (*$P < 0.05$, **$P < 0.01$).

nanocrystal size, where cancer cells preferentially adhered to36. We constructed an osteogenic niche-targeted nanoparticle with 50% DSS6 conjugation to specifically deliver therapeutic agents into the trabecular bone area with immature HA *in vivo*. The targeted nanoparticles preferentially bound to metaphyseal bone fragments rather than diaphyseal bone fragments. 50% DSS6 conjugation enriched nanoparticles in the trabecular bone of femur and tibia in mice.

It was found that the metastatic osteogenic niches were restricted in the trabecular bone with high bone anabolic activity, located near the growth plate cartilage in mice[8]. This phenomenon was also observed in the H&E staining images in this study. High bone mineral density correlated with the increased risk of bone metastasis in breast cancer patients[37]. Arsenic had the capability to reduce bone mineral density and trabecular bone volume of the femur by decreasing osteoblast mineralization in rats[14]. We demonstrated that *Runx2* and *Opn* genes in arsenic-treated MSCs and osteoblastic cells were greatly inhibited. *Runx2* drove the stage-transition of osteoblast phenotype and served a determinant function in bone formation[38]. Thus, it was speculated that arsenic treatment could reduce the available pre-metastatic sites for tumor cell colonization.

Arsenic trioxide has been approved for the treatment of acute promyelocytic leukemia and is also used as therapeutics of other hematopoietic malignancies in clinical studies[39]. We previously demonstrated that arsenic trioxide as niche-based therapeutic agents could remove the protection of vascular niches to primitive chronic myeloid leukemia cells in the bone marrow microenvironment[18]. In this report, we found that arsenic trioxide prevented DTC colonization in the osteogenic niche. However, arsenic trioxide has systemic toxicities and also disrupted the hematopoiesis in the bone marrow. Here, we entrapped As-Mn nanocrystals (around 14 nm) in biodegradable polymeric nanoparticles with a facile modified double emulsion (w/o/w) method developed in our laboratory. *In vivo* intravenous injection of As-Mn-containing nanoparticles effectively extended the survival of mice with 4T1 syngeneic bone metastasis. 50% DSS6 modified As-Mn nanoparticles showed superior therapeutic efficacy and reduced the bone marrow and hepatic toxicity of arsenic in normal mice.

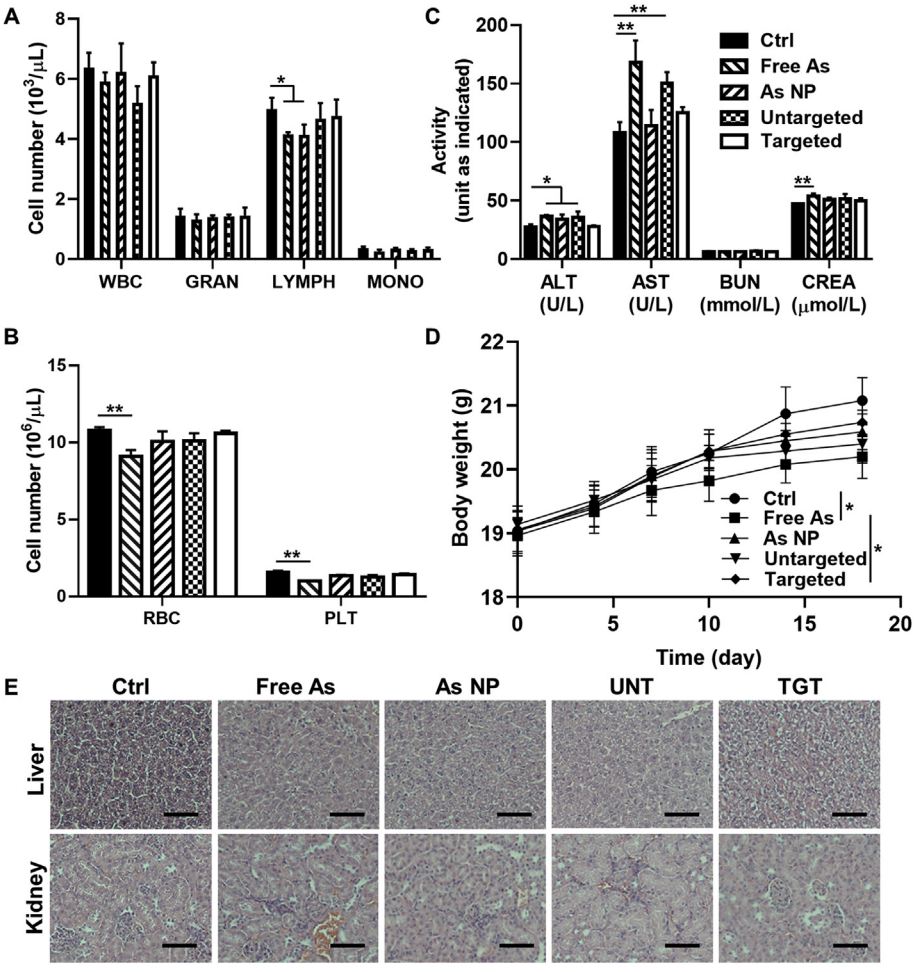

Figure 7 *In vivo* systemic toxicity after treatment with different arsenic formulations in normal BALB/c mice ($n = 4$). (A) Relative blood index of white blood cell (WBC), granulocyte (GRAN), lymphocyte (LYMPH), and monocyte (MONO). (B) Relative blood index of red blood cell (RBC) and platelet (PLT). (C) The levels of alanine aminotransferase (ALT), aspartate aminotransferase (AST), blood urea nitrogen (BUN), and creatinine (CREA). (D) Body weight changes of mice after intravenous injection of different arsenic formulations (*, for comparisons of indicated groups on Days 14 and 18). (E) Histopathological analysis of the liver and kidney after different treatments (scale bars = 500 μm). Data are presented as mean ± SD (*$P < 0.05$, **$P < 0.01$).

5. Conclusions

The 50% DSS6 peptide conjugated As-Mn nanocrystal containing polymeric nanoparticles were successfully prepared with excellent osteogenic niche targeting efficiency. Arsenic formulations can greatly reduce the adhesion ability of 4T1 cells to osteogenic cells and inhibit colony formation in the osteogenic cell-mimic bone marrow microenvironment. Arsenic also slowed breast bone colonization *via* altering the direct interaction between tumor cells and osteogenic cells and blocked the chemotactic migration of 4T1 cells toward osteogenic cells in the mimic 3D osteogenic niche. This resulted in remarkable therapeutic efficacy in the syngeneic murine model of breast tumor bone metastasis with no systemic toxicities to normal mice. In summary, we developed an osteogenic niche-targeted approach to enrich drugs in the subtissue in the bone marrow. This approach could selectively deliver arsenic into the local bone microenvironment to prevent tumor cell colonization and thereby be used for the treatment of bone metastasis.

Acknowledgments

The authors acknowledge financial support from the National Natural Science Foundation of China (81703713, 81774011, and 81673607), Engineering Research Center of Clinical Functional Materials and Diagnosis & Treatment Devices of Zhejiang Province (WIBEK181001, China), Natural Science Foundation of Zhejiang Province grants (Y19H280001, China), China Postdoctoral Science Foundation (2020M672882, China), and internal support from Zhejiang Chinese Medical University. We appreciate the great technical support from the Public Platform of Medical Research Center, Academy of Chinese Medical Science, Zhejiang Chinese Medical University.

Author contributions

Cong Liu and Anzhi Hu performed the research, analyzed data, and wrote the paper. Huijuan Chen participated part of the experiments. Jing Liang revised the manuscript. Mancang Gu and Yang Xiong provided technical and material support. Chao-Feng Mu conceptualized the project and revised the manuscript. All the authors have read and approved the final manuscript.

Conflict of interest

The authors have no conflicts of interest to declare.

Appendix A. Supporting information

Supporting data to this article can be found online at https://doi.org/10.1016/j.apsb.2021.06.012.

References

1. Croucher PI, McDonald MM, Martin TJ. Bone metastasis: the importance of the neighbourhood. *Nat Rev Cancer* 2016;**16**:373–86.
2. Weilbaecher KN, Guise TA, McCauley LK. Cancer to bone: a fatal attraction. *Nat Rev Canc* 2011;**11**:411–25.
3. Peinado H, Zhang H, Matei IR, Costa-Silva B, Hoshino A, Rodrigues G, et al. Pre-metastatic niches: organ-specific homes for metastases. *Nat Rev Cancer* 2017;**17**:302–17.
4. Rossnagl S, Ghura H, Groth C, Altrock E, Jakob F, Schott S, et al. A subpopulation of stromal cells controls cancer cell homing to the bone marrow. *Cancer Res* 2018;**78**:129–42.
5. Wang H, Yu C, Gao X, Welte T, Muscarella AM, Tian L, et al. The osteogenic niche promotes early-stage bone colonization of disseminated breast cancer cells. *Cancer Cell* 2015;**27**:193–210.
6. Shiozawa Y, Pedersen EA, Havens AM, Jung Y, Mishra A, Joseph J, et al. Human prostate cancer metastases target the hematopoietic stem cell niche to establish footholds in mouse bone marrow. *J Clin Invest* 2011;**121**:1298–312.
7. Devignes CS, Aslan Y, Brenot A, Devillers A, Schepers K, Fabre S, et al. HIF signaling in osteoblast-lineage cells promotes systemic breast cancer growth and metastasis in mice. *Proc Natl Acad Sci U S A* 2018;**115**:E992–1001.
8. He F, Chiou AE, Loh HC, Lynch M, Seo BR, Song YH, et al. Multiscale characterization of the mineral phase at skeletal sites of breast cancer metastasis. *Proc Natl Acad Sci U S A* 2017;**114**:10542–7.
9. Ren G, Esposito M, Kang Y. Bone metastasis and the metastatic niche. *J Mol Med (Berl)* 2015;**93**:1203–12.
10. Salamanna F, Borsari V, Pagani S, Brodano GB, Gasbarrini A, Fini M. Development and characterization of a novel human 3D model of bone metastasis from breast carcinoma *in vitro* cultured. *Bone* 2021;**143**:115773.
11. Wang H, Tian L, Liu J, Goldstein A, Bado I, Zhang WJ, et al. The osteogenic niche Is a calcium reservoir of bone micrometastases and confers unexpected therapeutic vulnerability. *Cancer Cell* 2018;**34**:823–39.
12. Hayashi T, Hideshima T, Akiyama M, Richardson P, Schlossman RL, Chauhan D, et al. Arsenic trioxide inhibits growth of human multiple myeloma cells in the bone marrow microenvironment. *Mol Cancer Ther* 2002;**1**:851–60.
13. Wu CT, Lu TY, Chan DC, Tsai KS, Yang RS, Liu SH. Effects of arsenic on osteoblast differentiation *in vitro* and on bone mineral density and microstructure in rats. *Environ Health Perspect* 2014;**122**:559–65.
14. Hu YC, Cheng HL, Hsieh BS, Huang LW, Huang TC, Chang KL. Arsenic trioxide affects bone remodeling by effects on osteoblast differentiation and function. *Bone* 2012;**50**:1406–15.
15. Pereira JA, Das P, Chaklader M, Chatterjee S, Basak P, Chaudhuri S, et al. Effects of inorganic arsenic on bone marrow hematopoietic cells: an emphasis on apoptosis and Sca-1/c-Kit positive population. *J Stem Cells* 2010;**5**:117–27.
16. Vernhet L, Morzadec C, van Grevenynghe J, Bareau B, Corolleur M, Fest T, et al. Inorganic arsenic induces necrosis of human CD34-positive haematopoietic stem cells. *Environ Toxicol* 2008;**23**:263–8.
17. Yarbrough DK, Hagerman E, Eckert R, He J, Choi H, Cao N, et al. Specific binding and mineralization of calcified surfaces by small peptides. *Calcif Tissue Int* 2010;**86**:58–66.
18. Fan L, Liu C, Hu A, Liang J, Li F, Xiong Y, et al. Dual oligopeptides modification mediates arsenic trioxide containing nanoparticles to eliminate primitive chronic myeloid leukemia cells inside bone marrow niches. *Int J Pharm* 2020;**579**:119179.
19. Zhu W, Wang M, Fu Y, Castro NJ, Fu SW, Zhang LG. Engineering a biomimetic three-dimensional nanostructured bone model for breast cancer bone metastasis study. *Acta Biomater* 2015;**14**:164–74.
20. Li B, Gu Z, Kurniawan N, Chen W, Xu ZP. Manganese-based layered double hydroxide nanoparticles as a T1 -MRI contrast agent with ultrasensitive pH response and high relaxivity. *Adv Mater* 2017;**29**:1700373.
21. Zhao Z, Wang X, Zhang Z, Zhang H, Liu H, Zhu X, et al. Real-time monitoring of arsenic trioxide release and delivery by activatable T1 imaging. *ACS Nano* 2015;**9**:2749–59.
22. Zhang G, Guo B, Wu H, Tang T, Zhang BT, Zheng L, et al. A delivery system targeting bone formation surfaces to facilitate RNAi-based anabolic therapy. *Nat Med* 2012;**18**:307–14.
23. Papaccio F, Paino F, Regad T, Papaccio G, Desiderio V, Tirino V. Concise review: cancer cells, cancer stem cells, and mesenchymal

stem cells: influence in cancer development. *Stem Cells Transl Med* 2017;**6**:2115−25.
24. Li XQ, Du X, Li DM, Kong PZ, Sun Y, Liu PF, et al. ITGBL1 is a *Runx2* transcriptional target and promotes breast cancer bone metastasis by activating the TGFbeta signaling pathway. *Canc Res* 2015;**75**:3302−13.
25. Waning DL, Guise TA. Molecular mechanisms of bone metastasis and associated muscle weakness. *Clin Cancer Res* 2014;**20**:3071−7.
26. Sabokbar A, Millett PJ, Myer B, Rushton N. A rapid, quantitative assay for measuring alkaline phosphatase activity in osteoblastic cells *in vitro*. *Bone Miner* 1994;**27**:57−67.
27. Tu Q, Zhang J, Paz J, Wade K, Yang P, Chen J. Haploinsufficiency of *Runx2* results in bone formation decrease and different BSP expression pattern changes in two transgenic mouse models. *J Cell Physiol* 2008;**217**:40−7.
28. Boskey AL, Spevak L, Paschalis E, Doty SB, McKee MD. Osteopontin deficiency increases mineral content and mineral crystallinity in mouse bone. *Calcif Tissue Int* 2002;**71**:145−54.
29. Celia-Terrassa T, Kang Y. Distinctive properties of metastasis-initiating cells. *Genes Dev* 2016;**30**:892−908.
30. Unnikrishnan D, Dutcher JP, Garl S, Varshneya N, Lucariello R, Wiernik PH. Cardiac monitoring of patients receiving arsenic trioxide therapy. *Br J Haematol* 2004;**124**:610−7.
31. Wan L, Pantel K, Kang Y. Tumor metastasis: moving new biological insights into the clinic. *Nat Med* 2013;**19**:1450−64.
32. Luo X, Fu Y, Loza AJ, Murali B, Leahy KM, Ruhland MK, et al. Stromal-initiated changes in the bone promote metastatic niche development. *Cell Rep* 2016;**14**:82−92.
33. Maes C, Kobayashi T, Selig MK, Torrekens S, Roth SI, Mackem S, et al. Osteoblast precursors, but not mature osteoblasts, move into developing and fractured bones along with invading blood vessels. *Dev Cell* 2010;**19**:329−44.
34. Hebert JD, Myers SA, Naba A, Abbruzzese G, Lamar JM, Carr SA, et al. Proteomic profiling of the ECM of xenograft breast cancer metastases in different organs reveals distinct metastatic niches. *Cancer Res* 2020;**80**:1475−85.
35. Werner-Klein M, Grujovic A, Irlbeck C, Obradovic M, Hoffmann M, Koerkel-Qu H, et al. Interleukin-6 trans-signaling is a candidate mechanism to drive progression of human DCCs during clinical latency. *Nat Commun* 2020;**11**:4977.
36. Pathi SP, Lin DD, Dorvee JR, Estroff LA, Fischbach C. Hydroxyapatite nanoparticle-containing scaffolds for the study of breast cancer bone metastasis. *Biomaterials* 2011;**32**:5112−22.
37. Cauley JA, Lucas FL, Kuller LH, Vogt MT, Browner WS, Cummings SR. Bone mineral density and risk of breast cancer in older women: the study of osteoporotic fractures. *J Am Med Assoc* 1996; **276**:1404−8.
38. Meyer MB, Benkusky NA, Pike JW. The *Runx2* cistrome in osteoblasts: characterization, down-regulation following differentiation, and relationship to gene expression. *J Biol Chem* 2014;**289**: 16016−31.
39. Liu JX, Zhou GB, Chen SJ, Chen Z. Arsenic compounds: revived ancient remedies in the fight against human malignancies. *Curr Opin Chem Biol* 2012;**16**:92−8.